NONLINEAR ROLL WITH WATER-ON-DECK: NUMERICAL APPROACH

V. L. Belenky, ABS, (USA), K. M. Weems, SAIC, (USA), D. Liut, SAIC, (USA),
Y.S. Shin, ABS, (USA)

Abstract

The paper describes the numerical analysis of the dynamics of a ship with green-water-on-deck using a time-domain prediction system that integrates 3-D wave-body hydrodynamics and the numerical solution of water-on-deck flow. The wave-body hydrodynamics are computed using a 3-D time-domain potential flow panel method based on a body-nonlinear formulation. The water-on-deck flow is computed using a concurrent time-domain solution driven by the relative motion of the ship and the incident wave at the deck edge and the motion of the deck. The predicted water-on-deck pressures are integrated and used directly in the calculation of the ship motions and loads. Several water-on-deck flow models are analyzed, including a finite-volume solution of the 3-D shallow-water flow equations, which is described in detail. This water-on-deck model can include bulwarks, freeing ports, and other deck features.

The main focus of the paper is the qualitative validation of the model, based on how well the model predicts known nonlinear behavior. The predicted rolling behavior of a 21-meter fishing vessel with various computational options is analyzed.

1. INTRODUCTION

While computer simulations of water-on-deck and deck-in-water problems can be viewed as a principal tool in both research and everyday design work, such simulations pose a challenge in interpreting results and their validity. Large ship motion with water-on-deck is a highly nonlinear phenomenon, which is prone to "strange" behavior. Therefore, a computational result that is unusual or unexpected may not necessarily be wrong. Conversely, a fit within an expected numerical range does not guarantee that the result is correct. This makes physical adequacy of simulation a central issue, even as computational effectiveness is being improved constantly due to increasing numerical power of hardware.

What could be considered a proper validation? Traditionally, since the time of Galileo, a hypothesis must be tested against experiments that are carried out in a manner aimed at rejecting the hypothesis; if the experiments fail, the hypothesis becomes a theory. However, computer simulation is – by its nature – in between experiment and theory. Even though the governing equations themselves might be beyond any doubt, the numerical realization of those equations is always approximate, which is a source for a number of inadequacies ranging from rounding errors to numerical instabilities caused, for example, by small differences. Simple theoretical solutions could be considered as a validation of a numerical scheme. Then, a software's ability to reproduce known behavior can be considered as the most

basic qualitative validation. This kind of validation is the focus of this paper.

What kind of behavior should be reproduced? The dynamic system describing a ship with water-on-deck is quite complicated. First, the water was delivered on deck because the deck edge was submerged. Since we are interested in a large quantity of water (enough to change the vessel's behavior and create a capsizing threat), we probably have to consider a large portion of deck to be submerged at some point. Secondly, following [1, 2] we must consider two situations: "deck-in-water" and "water-on-deck". These situations are different in the way the water creates force on the ship. In the deck-in-water case, hydrodynamic pressures create the force on a flat portion of the deck, a force that is especially strong when the ship moves against the wave. In the water-on-deck case, a heeling moment is created by shifting the mass of the green-water-on-deck including additional forces caused by in- and outflow of the water and, eventually, by dynamical pressures on deck structures caused by wave flow [3, 4, 5]. Mathematical formulation of the difference between these situations is yet another challenge to be met.

Even if one artificially excludes the deck-in-water situations and the water's in- and outflow in the water-on-deck situations, the phenomenon is still too complicated for theoretical solution. It is possible, however, to estimate motion stability at medium range of ship roll, if no bulwark is present [6].

Only if behavior of water-on-deck is considered as purely static (this allows consideration of a ship with negative initial GM) the complete picture of motion be revealed with methods of contemporary nonlinear dynamics, including Melnikov analysis [7, 8, 9]. Direct comparison of simulation results with the above theoretical models meets certain difficulties concerning calculation of invariant manifolds for the dynamical system that are not completely described with a system of ordinary differential equations. These difficulties might be overcome but this is beyond this paper's scope.

This paper focuses on the simplest qualitative validation of simulated ship motion with green-water and deck submergence, while trying to find simple physical explanation to the results of numerical simulation. This paper is direct development and inclusive update of the previous one [10].

2. COMPUTATIONAL SYSTEM OVERVIEW

The computational system used in the present study is the result of a recent effort to develop a sophisticated green-water-on-deck model that could be integrated directly into a time-domain ship motion calculation, thus allowing green-water effects to be included in the calculation of nonlinear ship motions and loads. In order to attain this, an approach was selected in which the ship motions and green-water-on-deck calculations run concurrently in the time domain. In effect, this approach subdivides the computational domain into an "outer" solution of the ship-wave interaction problem and an "inner" solution of the green-water-on-deck problem, as illustrated in Fig. 1.

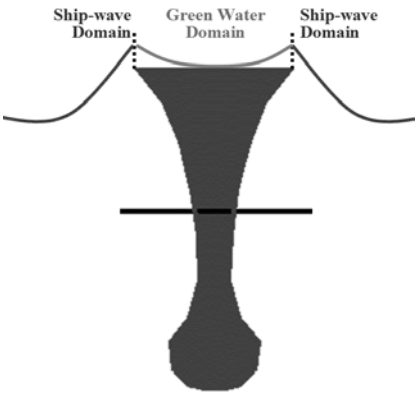

Fig. 1. Decomposition of the Computation Domain

The ship motions code in the present effort is the Large Amplitude Motions Program (LAMP) System. At each time step of the LAMP calculation, the ship motion and wave definition are used to compute the relative motion at the deck edge (often called the deck edge exceedance), the deck tilt, and the deck acceleration, which are then passed to the green-water-on-deck calculation. The green-water calculation is subsequently updated, after which the green-water pressure and forces are passed back to the ship motions calculation to be used in solving the equations of motions and computing sectional loads. The structure of this computational approach is illustrated in Fig. 2.

The integration of the green-water calculation in the LAMP System has been done in a "modular" fashion so that different "levels" of calculations are available. At the present time, three types of green-water calculations are implemented: the direction calculation of deck pressure from hydrostatics and incident wave (Froude-Krylov) pressure, a semi-empirical approach in which the green-water elevations are computed directly from the edge exceedance, and a solution of the shallow-water flow across the deck. The later model constitutes the principal focus of the present investigation. An additional computational approach, which eliminates the shallow-water assumption and solves the flow over the deck using a full 3-D finite volume method, is currently under development.

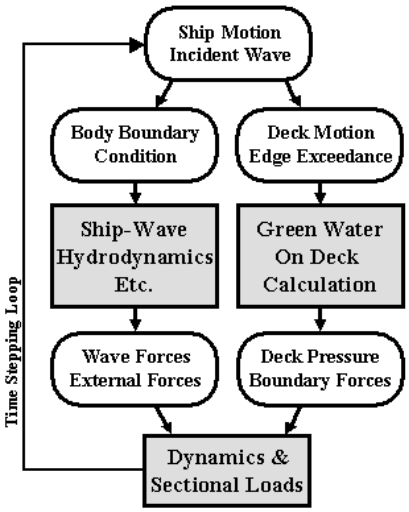

Fig. 2. Structure of the LAMP System with Green-Water-On-Deck

3. THE LAMP SYSTEM

The LAMP System is a time-domain simulation model specifically developed for computing the motions and loads of a ship operating in extreme sea conditions. The development of the LAMP System began with a 1988 DARPA project for advanced nonlinear ship motion simulation, and has continued under the sponsorship of the U.S. Navy, U. S. Coast Guard, the American Bureau of Shipping (ABS), and SAIC's IR&D program.

LAMP uses a time stepping approach in which all of the forces and moments acting on the ship, including those due to the wave-body interaction, appendages, control systems, and green-water, are computed at each time step and the 6-DOF equations of motions are integrated in the time-domain using a 4th-order Runge-Kutta algorithm. In addition to motions, LAMP also computes main girder loads using a rigid or elastic beam model and includes an interface for developing Finite-Element load data sets from the 3-D pressure distribution [11].

With its general nonlinear time-domain approach and solution of the 3-D flow field,

LAMP is well suited for incorporating a nonlinear green-water-on-deck calculation model.

3.1 Wave-Body Hydrodynamics

The central part of the LAMP System is the 3-D solution of wave-body interaction problem in the time-domain [12, 13]. A 3-D disturbance velocity potential is computed by solving an initial boundary value problem using a potential flow "panel" method. A combined body boundary condition is imposed which incorporates the effects of forward speed, ship motion (radiation), and the scattering of the incident wave (diffraction). The potential is computed using a hybrid singularity model that uses both transient Green functions and Rankine sources [14]. Once the velocity potential is computed, Bernoulli's equation can then be used to compute the hull pressure distribution including the second-order velocity terms. The disturbance velocity potential can be solved over either the mean wetted surface (the "body linear" solution) or over the instantaneously wetted portion of the hull surface beneath the incident wave (the "body nonlinear" approach). In either case, it is assumed that both the radiation and diffraction waves are small compared to the incident wave so that the free-surface boundary conditions can be linearized with respect to the incident-wave surface. Similarly, the incident wave forcing (Froude-Krylov) and hydrostatic restoring force can also be computed either on the mean wetted surface or on the wetted hull up to the incident wave.

The combinations of the body linear and body nonlinear solutions of the perturbation potential and the hydrostatic/Froude-Krylov forces provide multiple "levels" of solution of the ship-wave interaction problem. For most problems, the most useful of these is the "approximate body-linear" solution, which combines the body-linear solution of the disturbance potential with body-nonlinear hydrostatic-restoring and Froude-Krylov wave forces. This latter approach captures the significant nonlinear effects of most ship-wave problems at a fraction of the computation effort of the general body-nonlinear formulation.

3.2 Non-Pressure Forces

In additional to the calculation of the hydrodynamic pressure, LAMP includes models for non-pressure forces including viscous roll damping, propeller thrust, bilge keels, rudder and anti-rolling fins, mooring cables, and other systems. For oblique-sea cases, a PID (Proportional, Integral, and Derivative) course-keeping rudder control algorithm and a rudder servo model are implemented. Because of the time-domain approach, these non-pressure force models can include arbitrary nonlinear dependency on the motions, etc. Adjustable viscous roll-damping models are available that allow the roll damping to be "tuned" to match experimental values by simulating roll decay tests.

The non-pressure force model has also been used to integrate ship motions with crane pendulation, anti-rolling tank systems, and cargo sloshing models of various kinds. The cargo sloshing models, which are currently very simple, have been used to provide a simple evaluation of loss of stability for trapped water-on-deck.

3.3 Green-Water Interface

At each time step, LAMP uses the ship rigid body motion, the incident wave definition, and the hull pressure distribution to compute the relative motion of the edge of the deck to the wave surface. The hull pressure is used to predict the disturbance wave or "pile-up" of the free surface due to the presence of the ship. This relative wave height (or deck exceedance)

and its relative flow velocity are passed to the green-water-on-deck calculation module in order to define suitable inflow and outflow boundary conditions. The ship's rigid body motion, velocity, and acceleration vectors are also passed in order to define the tilt of the deck and inertial terms in the green-water-on-deck equations.

Based on these data, the green-water-on-deck calculation is then advanced to the current LAMP time calculation. The deck pressure and edge forces due to green-water are passed back to LAMP where they are integrated and added to the right hand side of the equations of motion as well as being used in the sectional-load calculations.

3.4 Applications And Validation

The LAMP System has been applied to a variety of conventional and unconventional ships and marine structures including naval combatants, tankers, bulk carriers, container ships, wave-piercing "tumblehome" ships, high-speed displacement multi-hulls, buoys, and the Navy's Mobile Offshore Base (MOB).

A number of LAMP validation studies have been performed, including an extensive series of calculation for the U.S. Navy CG-47 class cruiser in storm sea conditions (*e.g.*[11]). These studies have been instrumental in validation the ability of both the "body-nonlinear" and "approximate body-nonlinear" approaches to predict the nonlinear behavior of bending moments for flared-bow ships in extreme sea conditions

Another important validation study was the analysis of parametric rolling for a post-panamax containership in large head and following seas [15]. This study, which included computations using LAMP and other systems as well as extensive model tests, demonstrated that the LAMP System could capture both the incidence and magnitude of large roll motions excited by the nonlinear coupling between pitch and roll motions

4. GREEN-WATER CALCULATION

In the LAMP System, green-water effects are modeled using a concurrent, time domain calculation of the water-on-deck. The implementation is modular, with four different water-on-deck calculation options implemented or under development:

1. *Hydrostatic and Froude-Krylov pressure*: Deck pressure is computed from the submergence of each deck element and the linear incident wave pressure ($\partial\Phi/\partial t$). This is a straightforward modeling of the deck as a "body-nonlinear" hydrostatic/Froude-Krylov surface and represents the basic deck-in-water calculation.

2. *Semi-empirical model*: Water-on-deck is calculated directly from deck edge exceedance using an empirical expression derived from [16]. The resulting deck pressure, including the effects of the deck motion, can then be evaluated following the approach proposed by [17]. This model is intended to provide a quick estimate of the effect of foredeck green-water on ship motions and main girder loads.

3. *Shallow water flow calculation*: Computes the longitudinal and transverse flow over the deck with the assumption of shallow water using a finite-volume technique. This is the principal green-water calculation used in the present study and is described in detail below.

4. *Fully 3-D flow calculation*: Computes the flow over the deck, including vertical gradients, using a 3-D volume grid and a finite-volume technique. This is a new technique that is not yet fully working but illustrates a likely future path for green-water calculation methods.

4.1 Shallow Water Flow Calculation

The most sophisticated of LAMP's current green-water-on-deck calculation methods is the one based on the solution of the shallow water flow equations using a novel finite volume strategy. In this method, the equations of conservation of mass and momentum are solved in the time domain, shallow-water assumptions are made, and viscous effects are ignored except for a relatively simple deck friction term. The shallow water assumptions are that the fluid acceleration normal to the deck can be ignored while the tangential fluid velocity and pressure are assumed to be constant across the depth of water-on-deck [18]. These assumptions reduce the 3-D fluid domain to a 2-D computational domain. This method can handle a variety of boundary and initial conditions, and it is capable of supporting arbitrary motions and general geometries of a ship deck, including partial height walls (e.g. bulwarks), "infinite" walls (e.g. deckhouses), and stepped or raised section (e.g. hatch covers). This approach has been validated with available experimental data and has been successfully integrated with the LAMP System [19]

For this approach to be useful as an integrated part of the LAMP simulation, the green-water-on-deck calculation is required to be reasonably fast, robust, and capable of calculating the flow on a deck that is moving with large-amplitude six-degrees-of-freedom motions and exchanging water with the environment. Because of these requirements, a considerable portion of the effort in developing and implementing the numerical method has been spent in ensuring a stable and reasonable solution even when the assumptions of shallow water flow are stretched to their limits.

4.2 Conservation of Mass

Given a control volume CV and the corresponding control surface CS enveloping it, Reynold's Transport Theorem can be used to express the principle of conservation of mass as

$$\frac{dm}{dt} = \frac{\partial}{\partial t}\int_{CV} \rho \, dVol + \int_{CS} \rho \left(\mathbf{v}_r \bullet \mathbf{n}\right) dS = 0 \qquad (1)$$

where S is the surface of CS, Vol represents the volume of CV, ρ is the fluid density, t is time, m is the mass of fluid inside CV, $\mathbf{v}_r$ is the flow velocity on CS, and $\mathbf{n}$ is the normal-to-S unit vector given point wise on S $\left[\mathbf{n} = \mathbf{n}(x, y, z)\right]$.

The first step to solving the shallow-water problem with the present strategy is to divide the computational domain into a set of vertical hexahedral elements (close-volume elements with quadrilateral faces), which are contiguously connected, as shown in Fig. 3.*a*

As seen in this figure, each element e has a fluid elevation h_e, measured from the geometric center of the base of the corresponding hexahedral element to its top. Also, for each element, a characteristic area C_e is defined, which is the projection of the base area of element e onto a surface normal to the z axis, which contains the geometric center of the hexahedral's base. The vertical axis z is set to be parallel to the acceleration of gravity. The four lateral faces of each element are defined by the surfaces A_s. Note that these faces remain vertical in the global system as the deck tilts.

As shown in Fig. 3.*a*, the subscript q_s denotes the adjacent element q to side s of a given element e. If an element had a triangular base, one of its four side surfaces A_s would be collapsed to a line, a situation that is perfectly acceptable with the present method. The normal vectors to the lateral areas, $\mathbf{n}$, are always normal to the gravity vector.

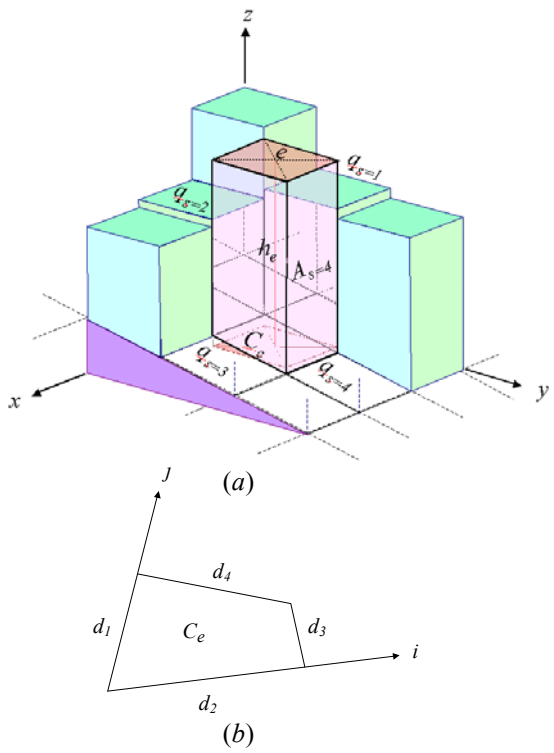

Fig. 3. Finite volume element e with adjacent elements q_s. The subscript s characterizes each of the four sides of element e. The corresponding numbering convention for s is given in part b, where the characteristic area C_e for a generic element e is shown, along with each side d_s.

The flow velocity measured on each lateral surface A_s is represented by the vectors $\mathbf{v}_r$, which are always parallel to the undisturbed water level. If the principle stated in equation (1) is applied to a generic element e, conservation of mass can be expressed as:

$$\frac{\partial}{\partial t}\left[\rho\ C\ h\right]_e + \left[\rho \sum_{s=1}^{4} \mathbf{v}_{r_s} \bullet \mathbf{n}_s\ A_s\ \right]_e = 0 \qquad (2)$$

where $\mathbf{v}_{r_s}$ is the average normal velocity to each lateral surface A_s of element e. Each element has a characteristic flow velocity $\mathbf{v}_e$ with horizontal components v_{x_e} and v_{y_e}.

As stated above, the platform for the shallow-water occurrence is allowed to move with six degrees of freedom following the deck of a ship. Thus, for each element, the base horizontal surface C_e will typically be a function of time. Regarding the differentials as finite differences and taking into account the incompressibility condition, equation (2) can then be written as:

$$\left[\overline{C}\ \Delta h\right]_e + \Delta t\left[\sum_{s=1}^{4}\left(\overline{v}_{r_x};\overline{v}_{r_y}\right)_s \bullet \left(\overline{n}_x;\overline{n}_y\right)_s\ \ \overline{h}_s\ \ \overline{d}_s\ \right]_e \cong 0 \qquad (3)$$

where the bars account for average values between time step k and k–1, and where d_s are the four sides s corresponding to the horizontal surface C_e (see Fig. 3.b). The subscripts x and y indicate vector components parallel to C_e in the corresponding x and y directions (see Fig. 3.a). Expanding the finite differences, equation (3) can be written as:

$$\left[\overline{C}^{k+1}\ \left(h^{k+1}-h^{k}\right)\right]_e + \Delta t\left[\sum_{s=1}^{4}\left(\overline{v}_{r_x};\overline{v}_{r_y}\right)_s^{k+1} \bullet \left(\overline{n}_x;\overline{n}_y\right)_s^{k+1}\ \ \overline{h}_s^{k+1}\ \ \overline{d}_s^{k+1}\right]_e \qquad (4)$$

where the superscript k is the time step counter. Rearranging terms and after some numerical treatment, equation (4) can be written in the compact form

$$M_{ee}^{j}\ h_e^{k_j+1} + \sum_{s=1}^{4} M_{eq_s}^{j}\ h_{q_s}^{k_j+1} = W_e^{j} \qquad (5)$$

where

$$M_{ee}^{j} = \left(\overline{C}^{k_{j-1}+1}\right)_e \qquad (6)$$

$$M_{eq_s}^{j} = \frac{\Delta t}{8} Q_{eq_s}^{k_{j-1}+1} \tag{7}$$

$$\begin{aligned} W_e^j = {} & h_e^k \, \overline{C}_e^{k_{j-1}+1} - \overline{\sigma}_{e_s}^{k_{j-1}-1} \, d_{eq_s} \, \Delta t \\ & - \frac{\Delta t}{4} \sum_{s=1}^{4} \left(Q_{ee_s}^{k_{j-1}+1} \, h_e^{k_{j-1}+1} + \frac{1}{2} Q_{eq_s}^{k_{j-1}+1} \, h_{q_s}^{k_{j-1}+1} \right) \\ & - \frac{\Delta t}{4} \sum_{s=1}^{4} \left(Q_{eq_s}^{k} h_{q_s}^{k} + Q_{ee_s}^{k} h_e^{k} \right) \end{aligned} \tag{8}$$

where

$$Q_{ee_s} = \left(v_x ; v_y\right)_e \bullet \left(n_x ; n_y\right)_{e_s} d_{e_s} \tag{9}$$

$$Q_{eq_s} = \left(v_x ; v_y\right)_{q_s} \bullet \left(n_x ; n_y\right)_{e_s} d_{e_s} \tag{10}$$

$$\overline{\sigma}_{eq_s} = \frac{2}{3} \sqrt{2 \, \gamma_e \left| \Delta \overline{\eta}_{eq_s} \right|} \, \Delta \overline{\eta}_{eq_s} \tag{11}$$

The variable γ_e is the vertical acceleration of element e (which is described in the next section), whereas $\Delta\eta_{qs}$ is the difference in fluid level between element e and element q_s. The superscript j is an iterative counter; an iterative process is needed to solve the algebraic equations defined by (5) since the coefficients defined by (7) and (8) are a function of the elevations h and the other two sets of unknowns given by the vectors **v**.

4.3 Conservation Of Momentum

Given a control volume CV, Reynold's Transport Theorem applied to the conservation of momentum principle yields the following formulation:

$$\begin{aligned} \frac{d(m\mathbf{v})}{dt} &= \frac{\partial}{\partial t} \int_{CV} \mathbf{v} \, \rho \, dVol + \int_{CS} \rho \, \mathbf{v} \left(\mathbf{v}_r \bullet \mathbf{n}\right) dS \\ &= \int_{CS} p \left(-\mathbf{n} \, dS\right) - \int_{CV} \rho \, \mathbf{b} \, dVol \end{aligned} \tag{12}$$

where **b** is a horizontal acceleration vector (described below), and p is pressure. If the same control volume defined for the conservation of mass formulation is considered for each element, and taking into account the incompressibility assumption, equation (12) can be written as:

$$\begin{aligned} & \left[\frac{\partial}{\partial t} \left[\mathbf{v} \, C \, h \right] + \sum_{s=1}^{4} \mathbf{v}_s \left(\mathbf{v}_{r_s} \bullet \mathbf{n}_s \right) A_s \right]_e = \\ & - \int_{CS_e} \gamma \, z \, \left(\mathbf{n} \, dS \right) - \int_{CV_e} \mathbf{b} \, dVol \end{aligned} \tag{13}$$

where γ is the vertical acceleration given by

$$\gamma = g + a_z \tag{14}$$

Thus the vertical acceleration γ includes the acceleration of gravity g and the vertical acceleration a_z induced by the vertical motion of the platform considered. The body accelerations represented by **b** are the horizontal accelerations (normal to the gravity vector) induced by the motion of the platform. Solving the integrals in equation (13), they yield

$$\begin{aligned} & \left[C \, h \frac{\partial \mathbf{v}}{\partial t} + \mathbf{v} \, h \frac{\partial C}{\partial t} + \mathbf{v} \, C \frac{\partial h}{\partial t} \right. \\ & \left. + \sum_{s=1}^{4} \mathbf{v}_s \left(\mathbf{v}_{r_i} \bullet \mathbf{n}_s \right) A_s \right]_e = \\ & - \left[\frac{\gamma}{2} \sum_{s=1}^{4} h_s^2 \, d_s \, \mathbf{n}_s + \mathbf{b} \, C \, h \right]_e \end{aligned} \tag{15}$$

Regarding the differentials as finite differences, equation (15) can be written as:

$$\begin{aligned} & \left[\overline{C} \, \overline{h} \, \Delta \mathbf{v} + \overline{\mathbf{v}} \, \overline{h} \, \Delta C + \overline{\mathbf{v}} \, \overline{C} \, \Delta h \right. \\ & \left. + \Delta t \sum_{s=1}^{4} \overline{\mathbf{v}}_s \left(\overline{\mathbf{v}}_{r_s} \bullet \overline{\mathbf{n}}_s \right) \overline{h}_s \, \overline{d}_s \right]_e \cong \\ & \left[- \frac{\overline{\gamma} \, \Delta t}{2} \sum_{s=1}^{4} \overline{h}_s^2 \, \overline{d}_s \, \overline{\mathbf{n}}_s - \overline{\mathbf{b}} \, \overline{C} \, \overline{h} \, \Delta t \right]_e \end{aligned} \tag{16}$$

where, as before, bars account for average values between time step k and k–1. Expanding the finite differences, this expression can take the following compact form:

$$R_{ee}^{j}\ \mathbf{v}_{e}^{k_j+1}+\sum_{s=1}^{4}R_{eq_s}^{j}\ \mathbf{v}_{q_s}^{k_j+1}=\mathbf{S}_{e}^{j} \tag{17}$$

where

$$R_{ee}^{j}=\left(\overline{C}_{e}^{k_{j-1}+1}\ \overline{h}_{e}^{k_j+1}+\overline{h}_{e}^{k_j+1}\ \Delta C_{e}^{k_{j-1}+1}+\overline{C}_{e}^{k_{j-1}+1}\ \Delta h_{e}^{k_j+1}\right) \tag{18}$$

$$R_{eq_s}^{j}=\frac{\Delta t}{2}\overline{D}_{s}^{k_{j-1}+1} \tag{19}$$

$$\mathbf{S}_{e}^{j}=\overline{C}_{e}^{k_j+1}\ \overline{h}_{e}^{k_j+1}\left(\mathbf{v}_{e}^{k}-\overline{\mathbf{b}}_{e}^{k_{j-1}+1}\Delta t\right)-\frac{\Delta t}{2}\sum_{s=1}^{4}\mathbf{v}_{q_s}^{k}\ \overline{D}_{s}^{k_{j-1}+1}-\overline{\mathbf{P}}_{e}^{k_j} \tag{20}$$

$$D_s=\frac{1}{2}\left(h_e\ d_{e_s}\ \overline{\mathbf{v}}_{r_e}\bullet\overline{\mathbf{n}}_{e_s}+h_{q_s}\ d_{e_s}\ \overline{\mathbf{v}}_{r_{q_s}}\bullet\overline{\mathbf{n}}_{e_s}\right) \tag{21}$$

The term $\overline{\mathbf{P}}_{e}^{k_j}$ is the force term due to the hydrostatic pressure, which is given by

$$\overline{\mathbf{P}}_{e}^{k_j}=\frac{1}{4}\overline{\gamma}_{e}^{k_{j-1}+1}\ \Delta t\sum_{s=1}^{4}\left(\overline{h}_{eq_s}^{2}\right)^{k_j+1}\overline{d}_{s}^{k_{j-1}+1}\ \overline{\mathbf{n}}_{s}^{k_{j-1}+1} \tag{22}$$

As in the case of the equations of mass, the system of equations defined by (17) is solved iteratively for **v** since the coefficients given by equations (18)-(22) are a function of **v** and *h*. In the overall scheme, at each iteration *j*, first the fluid elevations h_e are solved, next the *x* components of the vectors $\mathbf{v}_e$, followed by the *y* components of the same vectors. This process is repeated, within the same time step, until convergence is achieved.

4.4 Minimum Time Step

To attain stability in solving the conservation of momentum equations, the main diagonal of the corresponding set of algebraic equations must be predominant at all times. For the formulation proposed in this paper, the following conservative criterion was adopted:

$$\left|R_{ee}\right|>\operatorname{Max}\left|R_{eq_s}\right| \tag{23}$$

If the term ΔC_e in equation (18) is neglected, the previous criterion can be expressed as

$$C_e\ h_e^{k+1}+C_e\left(h_e^{k+1}-h_e^{k}\right)\ >\ \Delta t\ \operatorname*{Max}_{s}\left[\left(\sqrt{2\,\gamma_{\max}\ h_s}\right)d_s\ h_s\right]_e \tag{24}$$

where $\gamma_{\max}$ is the maximum value of the vertical acceleration (which includes the acceleration of gravity), and where $\sqrt{2\,\gamma_{\max}\ h_s}$ is an over-conservative estimate of the maximum velocity that could flow between two adjacent elements. Approximating C_e as $C_e=d_e\ d_s$, such as,

$$d_e=\min\left[\max\left(d_1,d_3\right),\max\left(d_2,d_4\right)\right] \tag{25}$$

where d_1, d_2, d_3, d_4 are the sides of C_e as defined in Fig. 3.*b* , then equation (24) can be written as:

$$\Delta t<\left(h_e^{k+1}-\left|\Delta h_e\right|\right)\frac{d_e}{\sqrt{2\,\gamma_{\max}}\ h_{\max}^{3/2}} \tag{26}$$

where $\Delta h_e=h_e^{k+1}-h_e^{k}$. The fluid elevation h_{max} is the maximum value of fluid elevation for the shallow-water assumptions to hold. A maximum value of Δh_e can be estimated using the conservation of mass equation (see equation (3)) as

$$C_e\left|\Delta h_e\right|<\Delta t\ \operatorname*{Max}_{s}\left[\left(\sqrt{2\ \gamma_{\max}\ h_s}\right)\ d_s\ h_s\right]_e \tag{27}$$

using similar assumptions as those for equation (24). If C_e is defined as $C_e=d_e\ d_s$, and using the concept of h_{max}, inequality (27) can be written as

$$\left|\Delta h_e\right|<\Delta t\ \frac{\sqrt{2\,\gamma_{\max}}\ h_{\max}^{3/2}}{d_e} \tag{28}$$

Replacing inequality (28) in (26), the latter yields

$$\Delta t < h_e^{k+1} \frac{d_e}{2\sqrt{2\gamma_{\max}}\, h_{\max}^{3/2}} \qquad (29)$$

Evidently, if h_e can take any value between zero and h_{max}, the only stable solution would be the trivial solution in which $\Delta t = 0$. Therefore, to render the calculation possible while at the same time stable, a minimum value of fluid level h_{min} must be defined such that when the fluid elevation of an element e drops below this value, that element should be considered dry. This minimum value will determine both the speed and the precision of the calculation. Equation (29) can be rewritten in terms of h_{min} as:

$$\Delta t < h_{\min} \frac{d_e}{2\sqrt{2\gamma_{\max}}\, h_{\max}^{3/2}} \qquad (30)$$

It remains to be determined what would constitute a good estimate for h_{max}. To this end, a suitable estimate for d_e must first be found. If the computational grid has elements such that their individual C_e areas are comparable, the ratio $d_e \cong L/N$ will be chosen as an estimate for the smallest value of d_e (which will determine the maximum time step to be used). The ratio L/N is computed as:

$$d_e = \underset{i,j}{\mathrm{Min}} \left(\frac{L_i}{N_i}, \frac{L_j}{N_j} \right) \qquad (31)$$

where L_i denotes lengths taken along the grid i directions, L_j designates lengths measured along the corresponding j directions (see Fig. 3), and where N_i is the i-wise grid dimension, whereas N_j is the j-wise grid dimension.

If h_{max} were arbitrarily small, Δt could take arbitrarily large values. But it is desirable that h_{max} be allowed to take the largest possible values to extend as much as possible the stable range for the computations of h_e. To this end, it is taken as a criterion that h_{max} be an order of magnitude larger than d_e. This criterion was chosen to be $d_e / h_{\max} \cong L/N^{1/2}$, which ensures that d_e is an order of magnitude smaller than h_{max}, whereas h_{max} is an order of magnitude smaller than L. This can be expressed as

$$h_{\max} = \varepsilon\, L = \frac{1}{\sqrt{N}} L \qquad (32)$$

$$d_e = \varepsilon^2 L = \frac{1}{N} L \qquad (33)$$

where

$$\varepsilon = \frac{1}{N^{1/2}} \qquad (34)$$

Replacing equations (32) and (33) into inequality (30), the latter yields

$$\Delta t < \frac{h_{\min}}{2} \frac{N^{-1/4}}{\sqrt{2L\gamma_{\max}}} \qquad (35)$$

which sets the maximum value of Δt that can be used to ensure a stable solution. The conditions required for this criterion can be summarized as:

- The individual area of each element of the computational grid must be of the same order of magnitude.
- The maximum fluid elevation $h_{\max} = L/\sqrt{N}$ should never be exceeded.
-

It can also be proven that the stability condition of inequality (35) deduced for the conservation-of-momentum is sufficient to satisfy the stability of the conservation-of-mass equations as well.

4.5 Boundary Conditions

At the edges of the deck, boundary conditions are applied by computing the volume flow through the side of the elements on the edge of the computational domain. This volume flow is computed from

- depth of the green-water on the element, h_e
- green-water velocity normal to edge, u_e
- height of the "external" wave relative to the deck edge (edge exceedance) , h_w
- normal component of velocity of "external" wave relative to deck, u_w
- bulwark height, h_b (if any)
- length of the element edge, l

For edges where both the green-water depth and the edge exceedance are below the bulwark height, the volume flow through the side will be zero. For cases without a bulwark or where either the green-water height or the edge exceedance is greater than the bulwark height, the edge velocity is computed as

$$\begin{aligned}\Delta h_e \cdot A_e = {} & u_w \cdot l \cdot \max(h_w - h_b, 0) \\ & - u_e \cdot l \cdot \max(h_e - h_b, 0) \\ & + \tfrac{2}{3}\sqrt{2g\Delta h} \cdot l \cdot \Delta h\end{aligned} \qquad (36)$$

Here, Δh is the signed effective height difference between the edge exceedance and green-water height, corrected for the presence of the bulwark:

$$\Delta h = \max(h_w, h_b) - \max(h_e, h_b) \qquad (37)$$

For most calculations involving bulwarks, it is desirable to model the holes in the bulwark, sometimes called "freeing ports," which allow trapped water-on-deck to escape. At the present time, the method does not have a "perforated bulwark" model, so a "drain" term is specified on the elements adjacent to bulwarks, which removes water from the edge elements at a rate proportional to the area of the freeing ports:

$$\Delta h_e \cdot A_e = A_{fp}\sqrt{2gh_e} \qquad (38)$$

This drain model does not consider the effect of the "external" water heights or velocity, but does provide a reasonable simulation of the freeing ports until a more suitable model can be implemented.

4.6 Testing and Validation

In order to test and validate the numerical solution of the shallow water calculation, computational studies have been made for several configurations for which detailed theoretical and experimental data are available. One such study examined the "dam-breaking" problem, which examined evolution of the level of water behind a dam after the dam is suddenly removed. A second study examined the outflow from a box whose end is suddenly removed. Both studies show good agreement between the present method and published data [19].

In order to test the implementation of the green-water calculation in the LAMP System, a series of calculations were made for the CG-47 cruiser, a U.S. Coast Guard Cutter, and a large modern container ship. Figure 4 shows a snapshot for the simulation of the container ship in very large oblique waves. These calculations have provided a qualitative validation of the system but have stopped short of a full quantitative validation due to the lack of detailed experimental green-water-on-deck data. However, some level of qualitative validation can be gleaned by comparing the result of the different green-water calculations to each other and to the statistics from which the semi-empirical model was derived. The qualitative validation continues with the fishing boat study described below.

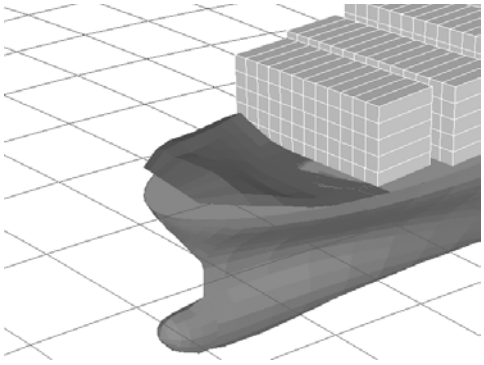

Fig. 4. Predicted Green-water for Container Ship in Severe Oblique Seas

5. FISHING BOAT CALCULATIONS

5.1 Configuration

The fishing vessel analyzed in the present study is the 21-meter stern dragger *Italian Gold*, which sank in heavy seas off Massachusetts in 1994. All calculations were made at a heavily loaded condition with a displacement of 197 tones and the center of gravity 0.08 meters above the mean waterline. The resulting transverse metacentric height (GM_t) is 0.22 m. The basic geometry model used in the hydrodynamic and hydrostatic calculations is shown in Figure 5.

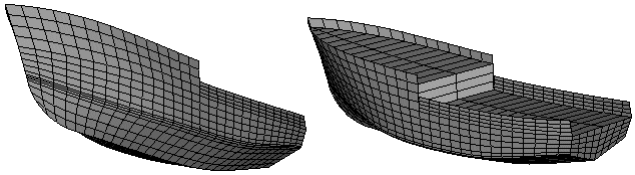

Figure 5. Fishing Boat Geometry

In the simulations, the skeg and rudder were modeled using "non-pressure" force models, so their effect was included in the solution of the equations of motions but not in the calculation of the wave-body interaction potential. Green-water-on-deck was calculated over the after deck, with inflow/outflow allowed over both sides and the stern of the ship.

All of the calculations in the present study were performed using LAMP's "approximate body-nonlinear" hydrodynamics model, in which the disturbance potential is computed over the mean wetted hull surface while the hydrostatic restoring and Froude-Krylov forces were computed of the instantaneously wetted portion of the hull beneath the incident wave.

5.2 Roll Decay Study

The first and, to this point, most extensive portion of the study has involved a series of roll decay calculations using different computational models and options. For clarity, these calculations were made in calm water at zero speed with the ship free only to roll. The initial roll angle was 30 degrees, at which the deck edge and bulwark are reasonably deeply submerged. For the case involving the shallow water green-water calculation, the deck elevations were initialized with stationary water-on-deck up to the calm waterplane Z=0. An initial calculation was made for the boat with no calculation of any kind on the afterdeck. A time history of the roll angle, in degrees, is shown in Figure 6. The "square-tooth" at the bottom of the upper graph indicates the relative motion of the "minimum freeboard point" of the deck edge – a high value indicates that the deck edge is submerged while a low value indicates that it is above the wave surface. This point, which is located just aft of the deckhouse, submerges at about 10° roll angle in calm water. To some extent, this indicates the beginning of the transition from "water-on-deck" to "deck-in-water."

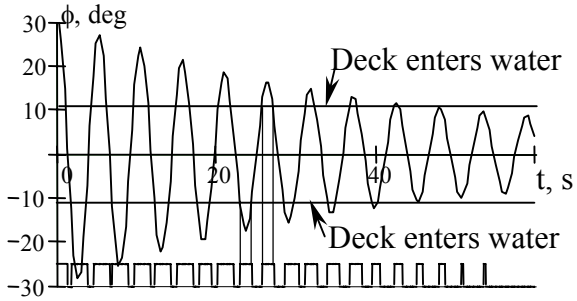

Figure 6. Roll Decay Angle and Deck Edge Submergence without Effect of Water on Deck

The initial roll period is 5.17 seconds and increases slightly to 5.47 seconds as the roll angle decreases. This change in roll period is due primarily to the change in hydrostatic restoring moment of the "body-nonlinear" formulation.

A second calculation computed water-on-deck pressure from hydrostatics, which corresponds to green-water calculation option 1 in Section 4 above. The results for this calculation are shown in Figure 7. In addition to the roll angle and deck edge submergence shown in the bottom graph, the top graph shows the volume of water-on-deck and a the resulting heeling moment. Since the model contains no "lag" of the water entering or leaving the deck, the volume of water and the heeling moment are exactly in phase with the roll angle. In other words, only the "deck-in-water" situation is modeled. The initial roll period increases to 5.96 seconds, an effect caused by the water-on-deck heeling moment, which in this case effectively decreases the restoring moment when the deck is submerged. As the roll angle decreases, the roll period decreases to 5.47 seconds, matching the period from the previous calculation.

A small but noticable decrease in the roll damping can be observed over the early portion of the run, where the longer roll period has decreased the roll velocity and reduced the damping due to skin friction and appendages.

Calculations were also made using the semi-empirical green-water-on-deck. Since the water-on-deck elevation is also exactly in phase with the deck edge motion, the results, which are not shown here, are very similar to the hydrostatic deck pressure results, although the empirical "correction" factor slightly reduces the water-on-deck volume and heeling moment.

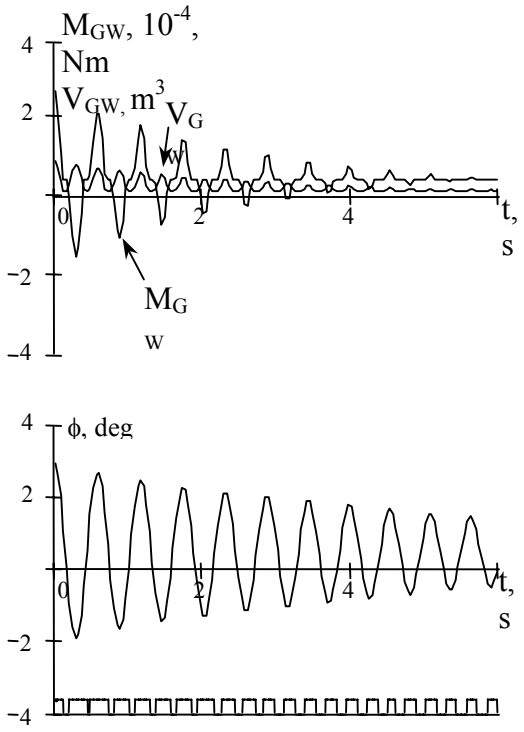

Figure 7. Roll Decay Results Including Hydrostatic Forces on Deck: Water-on-deck Volume (V_{GW}, top) and Roll Moment (M_{GW}, top), Roll Angle (□bottom), and Deck Edge Submergence (bottom)

The next calculation uses the finite-volume solution of the shallow water flow over the deck with a bare deck edge (*i.e.* no bulwark). The volume of water-on-deck starts out fairly large (as noted above, the finite-volume model is initially "full" to mean Z=0) and generally decreases as the water flows off the deck, although there are small periods of inflow during subsequent deck edge submergences.

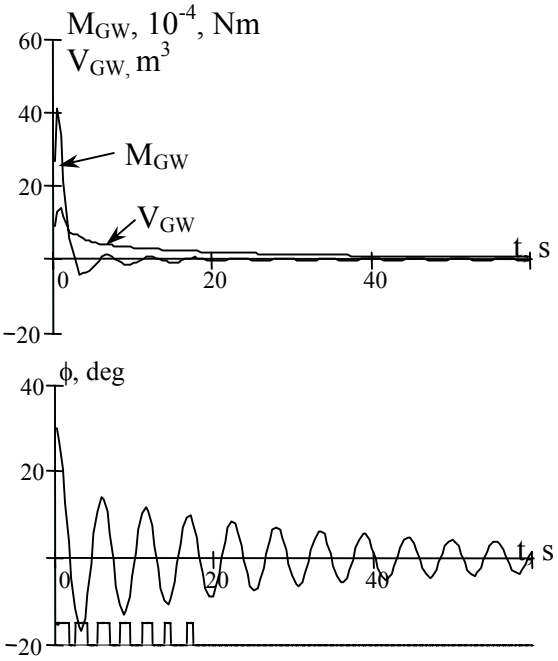

Figure 8. Roll Decay Results Including Finite-Volume Water-on-deck Effect Without Bulwarks

The initial roll period is similar to the hydrostatic pressure case, which is reasonable as the water-on-deck heeling moment is similar, while subsequent roll periods match both of the previous calculations at similar roll angles. Influence of water-on-deck and deck-in-water is realized mainly in a significant increase of roll damping.

Since the problem is otherwise nearly identical to that of the previous calculation, the damping influence must be credited to the water-on-deck. The most likely explanation is that the "lag" of the water flowing off the deck or to the other side of the boat when the boat rights itself results in a significant volume of water on the "rising" side of the deck, where the resulting deck pressure produces a significant moment in phase with but opposing the roll velocity. Evidence for this interpretation is offered in Figure 9, which shows a snapshot of the boat, which was initially heeled to starboard, with the computed water-on-deck surface as it rolls through 0° heel in the first cycle of the calculation. The extensive use of this type of visual simulation of the ship motion and water-on-deck has proved invaluable in both "debugging" the integrated green-water calculation and interpreting the results.

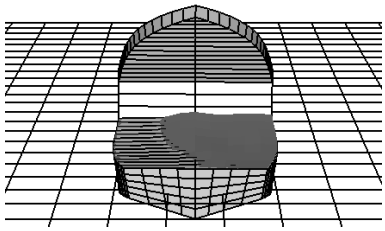

Figure 9. Computed Water-on-deck Surface for Boat as it Rolls Though 0 Heel

If confirmed, this result could offer an alternate source for the damping attributed by some sources to vortex shedding from deck edge or bulwark. In order to confirm this result, however, further investigation is clearly required, in particular relating to validation of the shallow-water flow model for the moving deck problem and an evaluation of the effect of the selected numerical parameters (especially grid size, time step, and minimum elevation) on the results.

The next calculation, whose results are shown in Figure 10, introduces a solid (no freeing ports) bulwark with height 0.853 m to the finite-volume calculation. The bulwark, which traps the water-on-deck and raises the angle at which water can enter the deck in calm water to over 20 degrees, changes the whole picture of motions. Damping is such that the second peak of roll angle is too small to immerse the bulwark top or to allow significant inflow. The amount of green-water stays constant and the ship quickly assumes a static heel angle of about 7 degrees.

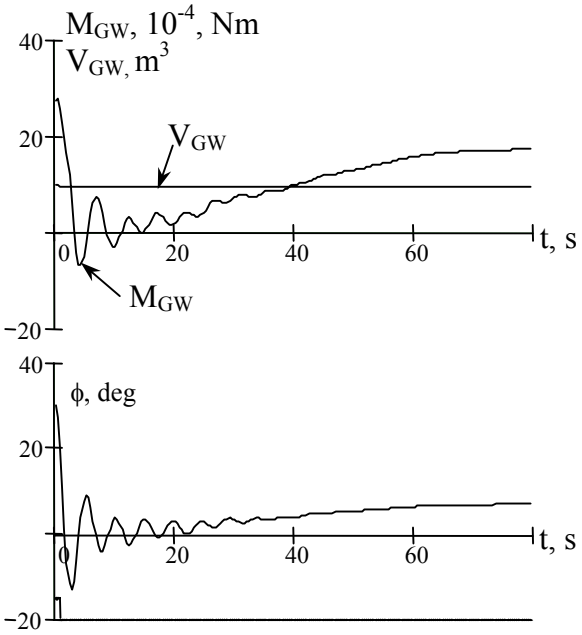

Figure 10. Roll Decay Results Including Finite-Volume Water-on-Deck Calculation with 0.853 m Bulwarks

5.3 Regular Wave Calculation

The second portion of the fishing boat study involved calculations for the boat at zero speed in regular (single frequency) beam waves. As in the roll decay test, the boat was free only to roll. While not exactly a realistic situation, it simplifies the comparison of the different calculations and reduces the risk of capsize, especially during the initial transient period. The wave height was 3.05 m (10 ft) with the period of 6.28 s, which makes the wave forcing close to the roll resonance regime. We wish to consider only the steady state rolling in the present discussion, so the results shown in Figures 11-14 are plotted beginning 520 seconds into the simulations. The initial transient behavior, which is both interesting and very important, is simply beyond the present scope of the work.

ϕ, deg

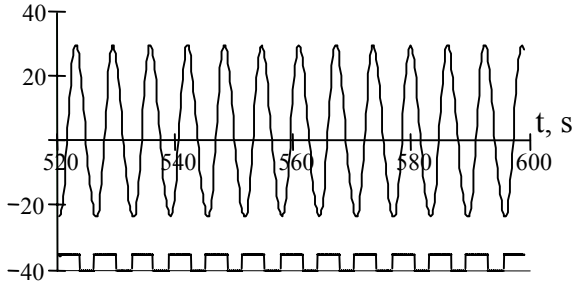

Figure 11. Regular Wave Roll without Effect of Water on Deck

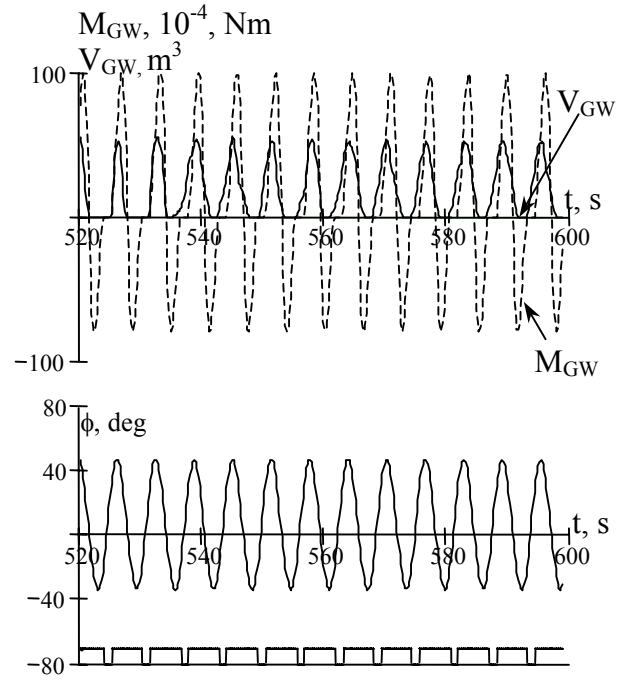

Figure 12. Regular Wave Results Including Hydrostatic Forces on Deck: Water-on-deck (V_{GW}, top) and Roll Moment (M_{GW}, top), Roll Angle (ϕ, bottom), and Deck Edge Submergence (bottom)

Figure 11 shows the results of the regular wave calculation for the boat with no deck model at all. The response has quite large amplitudes, which constitutes its nonlinear character. As for the roll decay results, the "square-tooth" indicates the submergence of the deck's, minimum point, which now is a function of the roll angle and the incident wave elevation

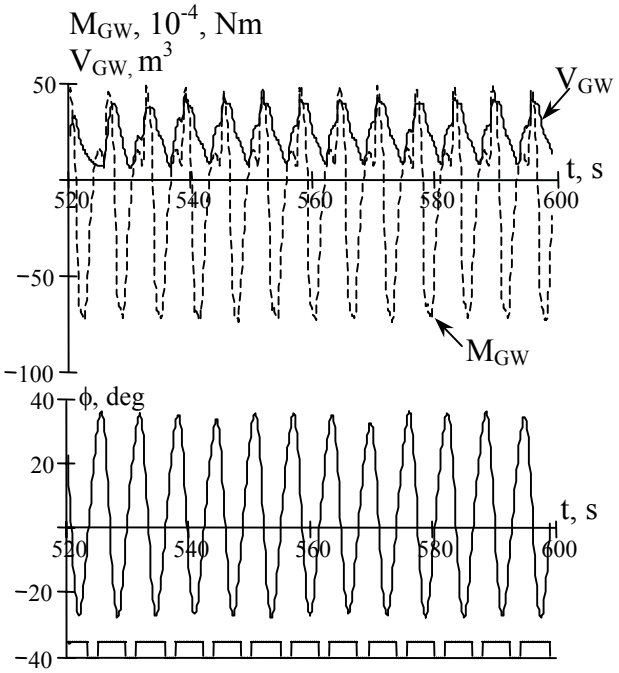

Figure 13. Regular Wave Results Including Finite-Volume Water-on-deck Calculation but no Bulwark

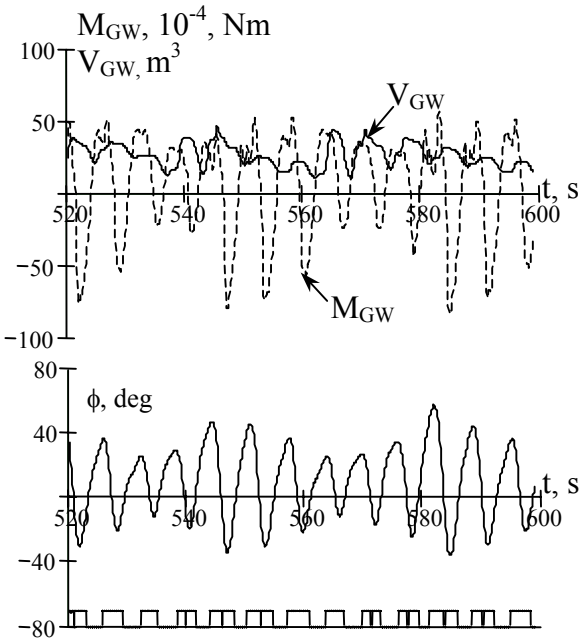

Figure 14. Regular Wave Results Including Finite-Volume Water-on-deck Calculation With 0.853 m Bulwarks

Figure 12 shows the results of the regular wave calculation with the deck pressure calculated as the hydrostatic and linear incident wave (Froude-Krylov) pressure only. The response is regular and primarily periodic at the forcing frequency. An increase in roll amplitude, attributed mostly to the decrease in restoring moment and rise in wave forcing when the deck is submerged, leads to an increasing amount of time "deck-in water"

The next regular wave calculation used the finite-volume calculation of the shallow water flow over the deck with bare deck edges (no bulwark), see fig. 13. The volume of water-on-deck, plotted on the top graph, changes by ~80% over the wave cycle. The roll response is smaller than the previous calculation, likely due to the water-on-deck damping seen in the roll decay study, and shows a bias of about 5° toward the "up-wave" direction. A weak subharmonic response can be observed.

Figure 14 shows the regular wave results with a 0.843 m bulwark added to the finite-volume calculation. The maximum volume of water-on-deck is just a bit higher than the no bulwark calculation, but the mean value has been substantially increased. A subharmonic response and increased roll amplitudes are observed.

Comparing Figures 13 and 14, a conclusion can be drawn that accumulation of water-on-deck has a major impact on ship dynamics: the subharmonic character of the response might be attributed to water-on-deck influence. Garkavy [20] reported subharmonic rolling of a ship with small freeboard (and as a result with water-on-deck) observed during model tests.

Observed subharmonic roll could be a result of period-doubling bifurcation, which is known to happen for nonlinear rolling in beam seas; see, for example, [21]. Accumulation of water-on-deck leads to a decrease of the instantaneous restoring moment. As a result, ship roll could

be shifted close to the nonlinear region in the vicinity of the GZ curve's peak, which might facilitate the bifurcation of the periodic solution.

However, in order to state that the observed behavior is the manifestation of period-doubling bifurcation, it is necessary to analyze the stability of steady state motion, which is beyond of the scope of the preliminary study presented here.

At the same time, the above consideration could be seen as a possible physical explanation of the observed results and as an indicator of validity for the described numerical model of water-on-deck.

5.4 Roll Response *vs.* Wave Frequency

The third portion of the study focused on how the steady-state roll response, including green-water effects, changes with the wave frequency. In order to clearly see the variation of the ship's steady-state behavior with frequency, a sequential series of simulations were performed in which the frequency was varied from well below the roll frequency, where the roll response was expected to be similar a linear prediction, through the regime of resonant rolling and ending with a high frequency, where the roll response was again expected to be more-or-less linear. For each frequency, the amplitude and phase of the steady-state rolling was evaluated. In order to minimize the transition process in the calculation, the steady-state values from each frequency was used to set initial conditions for the next. Such approach however should be considered as approximate [22], since it could not reproduce the wave disturbance pattern from the previous run. As a result, the transition process still took place but was much shorter than for a run starting from static heel.

In order to evaluate the dependence of the response on initial conditions, two sequences of frequencies were evaluated; from low to high (0.6 to 1.6 1/s) and from high to low (1.8 to 0.8 1/s). This analysis technique is quite commonly used when the dynamical system of interest is suspected of being capable of a fold bifurcation. Figure 16 shows the roll response curve for a wave amplitude of 0.6 m, calculated without including the effect of green-water.

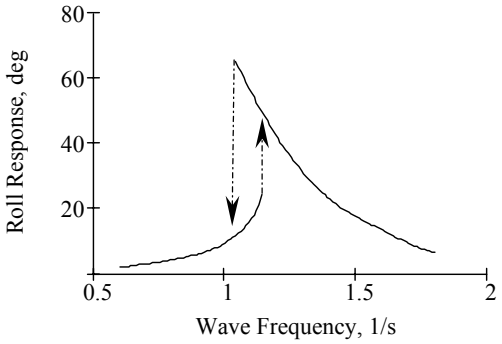

Figure 15. Roll response without green-water. Wave amplitude 0.6 m

Figure 15 clearly shows hysteresis: there is a range of frequencies where two stable steady-state responses exist depending on the initial conditions. It is possible to show [21] that the system experiences fold bifurcation.

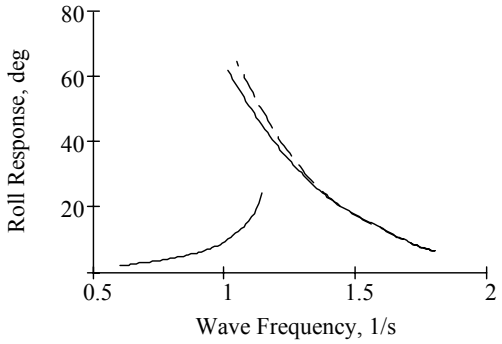

Figure. 16. Roll response with hydrostatic green-water effect (solid) compared to roll response with no green-water effect (dashed).

Figure 16 compares the roll response with the hydrostatic model of green-water (solid line) to the results without green-water (dashed line).

The green-water leads to slight decreasing of the roll amplitude near resonance. A plot of the volume of green-water on deck (see figure 17) also shows an area with two values for the same frequency.

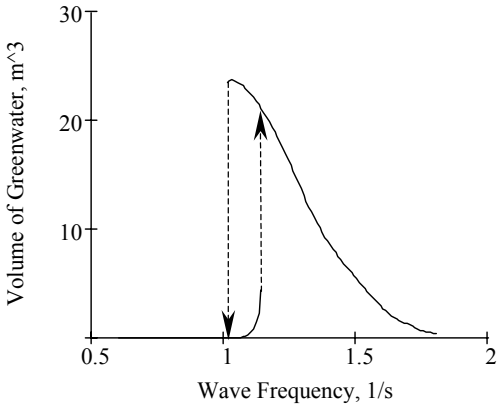

Figure 17. Max volume of green-water (hydrostatic model)

Not surprisingly, the volume of water on deck depends on roll response: areas of low roll have little water-on-deck and visa-versa. Figure 19 shows an analogous picture for the heeling moment created by the green-water.

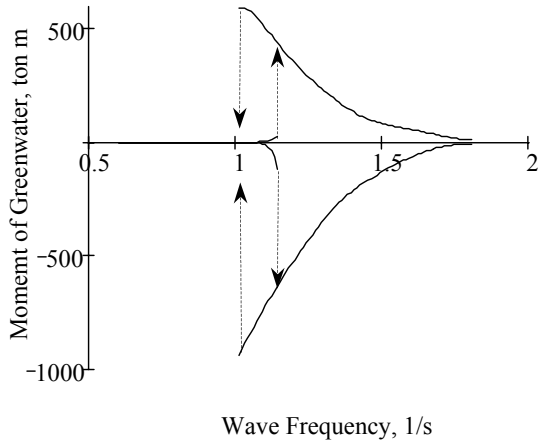

Figure 18 Extremes of moment created by the green-water (hydrostatic model)

Figure 18 also shows that there is significant asymmetry in the green-water moment: This appears to be related to the evident fact that the weather side is more exposed to the incoming wave than the lee side.

The hydrostatic model of green-water does not include any inertia of the water itself, so as the ship's deck edge rolls out of the water, the green-water immediately leaves the deck. The finite volume green-water model accounts for inertia of the water on deck and leads to dramatic changes in the roll response (Figure 19), including a significant reduction of the maximum roll angle near resonance.

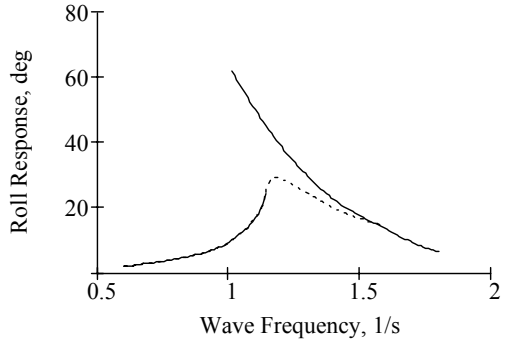

Figure 19. Roll response with finite volume model of green-water (dotted) vs. hydrostatic green-water model (solid)

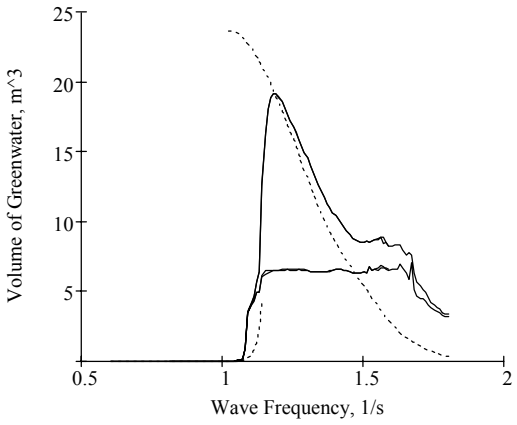

Figure 20. Minimum and maximum volume of green-water calculated with finite volume model (solid) vs. maximum volume of green water calculated with hydrostatic model (dotted)

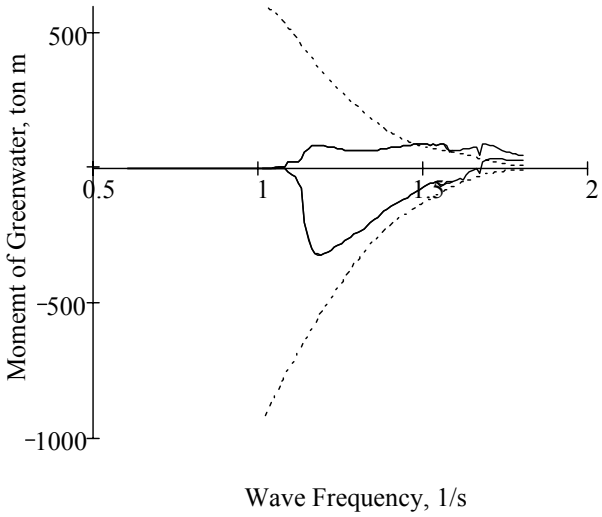

Figure 21. Extremes of green-water moment calculated with finite volume model (solid) vs. extremes of green-water moment calculated with hydrostatic model (dotted)

The minimum and maximum volume of green-water (Figure 20) also changes in comparison with the hydrostatic model. The maximum volume is smaller at low frequencies and larger at high frequencies as water on the deck is heavy and cannot leave the deck instantly as it does for the hydrostatic value. Also, a certain amount of green-water always stays on deck, so the minimum volume is not zero as it is for the hydrostatic model. It is interesting to note that the minimum volume stays almost constant through the resonant frequencies. Both minimum and maximum volume curves experience some high-pitch oscillations in relatively high-frequency range. Such changes of the volume might be attributed to dynamic effects of green-water, which might be more pronounced at higher frequencies.

Similar behavior can be observed for the high frequency range of the curve of extreme green-water moments (Figure 21). The low-frequency portion of these curves is similar to heel moments of the hydrostatic model (Figure 18) over to the low branch of roll response. This might be explained by the fact that the low-frequency motions result in smaller accelerations and inertial component might not be as significant. As the frequency increases, acceleration increases and the inertial forces of water on deck seem to prevent the system from performing a jump to high amplitude mode. It might be related to the same effect that is used in anti-rolling devices.

The introduction of a 0.8 m bulwark further changes the ship's behavior, as shown in Figures 22-24.

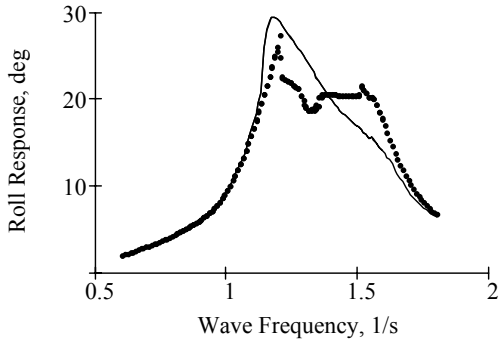

Figure 22. Roll response for finite-volume green-water model with 0.8 m bulwark (dotted) vs. with the same without the bulwark (solid)

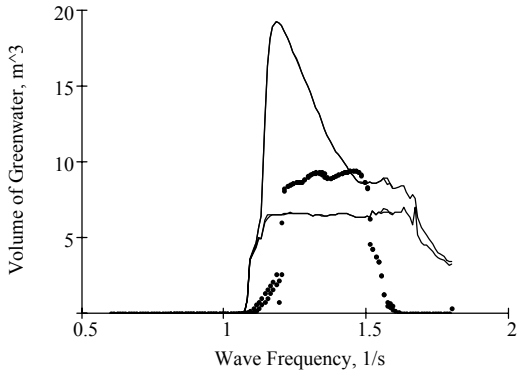

Figure 23. Minimum and maximum volume of finite-volume green-water model with 0.8 m bulwark (dotted) vs. with the same without the bulwark (solid)

The most noticeable feature of the calculation with the bulwark is an almost constant volume of the green-water (Figure 23) over the range of frequencies fro which the steady-state rolling amplitude is above about 20 degrees, which is the angle of deck well flooding. A

small peak of the roll response can been seen just below the roll natural frequency, immediately followed by minimum right after it (Figure 22).

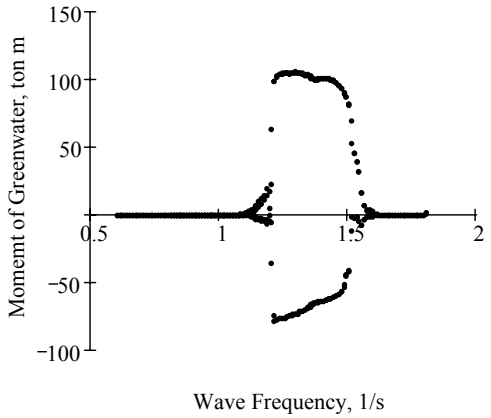

Figure 24. Extremes of green-water moment calculated with 0.8 m bulwark based on finite volume model of green-water

These peaks might be result of the internal motion of the water-on-deck. The very small peak of roll response in the high frequency range is probably the result of splashing the green-water out of deck well caused by increased (due to high frequency) inertial forces. In general, the frequency range where green-water behavior is observed is smaller than for case with no bulwark, since the bulwark increases the roll angle when the deck might be flooded.

Concluding here consideration of ship and green-water behavior in frequency domain, we would like to note the significant influence of inertial forces.

6. CONCLUSIONS

A computational simulation system for predicting ship motions, including the effects of green-water-on-deck, has been developed by integrating a series of water-on-deck models into a nonlinear time-domain ship motion computer simulation. These models include both a simple calculation of the deck-in-water effects using hydrostatic and Froude-Krylov pressure and an advanced finite-volume calculation of the flow of water over the deck with the assumption of shallow water. In the present simulation, the option for modeling the deck in the calculation is selected *a priori*. A more general approach to the problem may be to allow the calculation to shift between models as the problem changes from deck-in-water to water-on-deck. Such an approach presents many technical challenges, of course, but may be the appropriate framework for future development in this area.

Nevertheless, a study of the rolling behavior of a 21-meter fishing vessel seems to indicate that the present system is able to capture two major phenomena associated with water-on-deck and deck-in-water situations and known from experiments. The first is associated with increased damping caused both by the flow of water over the deck and the influence of the deck entering the water.
The second phenomenon is associated with subharmonic regular roll response of a ship with periodic immersion of the deck and an accumulation of green-water. This type of behavior, which has been previously observed in model tests, could be physically explained by the present results.

A series of systematical simulations of the roll motion vs. wave frequency and a comparison of hydrostatic green-water model to the finite volume green-water suggesting that the inertia of the water-on-deck plays a significant role in the ship's rolling behavior.

While the present analysis stops well short of constituting a validation study, the observation of these phenomena helps to suggest that the present model of nonlinear ship motion with water-on-deck is qualitatively reasonable. At the same time, the authors understand that this only represents an initial proof of adequacy and that rigorous validation and testing are required.

7. ACKNOWLEDGEMENTS

The development of the LAMP System has been supported by the U.S. Navy, the Defense Advanced Research Projects Agency (DARPA), the U.S. Coast Guard, the American Bureau of Shipping (ABS), and SAIC. The green-water development has been supported by the Office of Naval Research (ONR) under program manager Dr. Patrick Purtell, by the US Coast Guard under the Program manager Mr. Peter Minnick, and by ABS. The authors also wish to thank the manager of SAIC's Ship Technology Division, Dr. Woei-Min Lin.

8. REFERENCES

[1] Grochowalski, S., "Investigation into the Physics of Ship Capsizing by Combined Captive and Free-Running Model Tests," *SNAME Transactions,* pp 169-212. 1989

[2] Grochowalski, S., "Effect of Bulwark and Deck Edge Submergence in Dynamics of Ship Capsizing," *Proceedings, US Coast Guard Vessel Stability Symposium*, New London, Connecticut, USA, March 1993.

[3] Adee, B. and Caglayan, I., "The effect of free water on deck on the motions and stability of vessels," *Proc. of STAB'82: 2nd International Conference on Stability of Ships and Ocean Vehicles*, Tokyo, pp. 413-426, 1982.

[4] Amagai, K., Kimura, N. and Ueno, K., "On the Practical Evaluation of Shallow Water Effect in Large Inclination for Small Fishing Boats," *Proc. of STAB'94: 5th International Conference on Stability of Ships and Ocean Vehicles*, vol. 3, Melbourne, Florida, 1994.

[5] Grochowalski, S., Hsiung, C.C., Huang, Z.J. and Cong L.Z., "Theoretical modeling of ship motions and capsizing in large and steep waves," *Transactions SNAME,* Vol. 106, pp. 241-267, 1998.

[6] Garkavy, V. V., "On stability of steady state rolling being accompanied with the deck immersion," *Transactions of Kaliningrad Institute of Technology* "Seakeeping and Design of Fishing Vessels", Kaliningrad, pp. 56-62 (in Russian), 1985.

[7] Falzarano, J. M., Shaw, S. W. and Troesch, A.W. "Application of global methods for analyzing dynamical systems to ship rolling motion and capsizing", *International Journal of Bifurcation and Chaos,* Vol. 2, No 1, pp. 101-115, 1992.

[8] Kan, M., and Taguchi, H. "Chaos and fractals in loll type capsizing equation" *Transactions of West-Japan Society of Naval Architects* No 83, pp. 131-149. (in Japanese), 1992.

[9] Kan, M. and Taguchi, H. "Chaos and fractals in nonlinear rolling and capsize of a damaged ship", *Proc. of OTRADNOYE'93: International Workshop on the Problems of Physical and Mathematical Stability Modelling* Vol. 2, Paper No 2, Kaliningrad Institute of Technology, Kaliningrad, 1993

[10] Belenky, V.L., Liut D, Weems, K.M. and Shin, Y.S. "Nonlinear Ship Roll Simulation with Water-on-Deck", *Proc. of the 6th International Stability Workshop,* Web Institute, N.Y., U.S.A. 2002

[11] Weems, K., Zhang, S., Lin, W.M., Shin, Y.S, and Bennett, J., "Structural Dynamic Loadings Due to Impact and Whipping," *Proceedings of the Seventh International Symposium on Practical Design of Ships and Mobile Units*, The Hague, The Netherlands, 1998

[12] Lin, W.M., and Yue, D.K.P., "Numerical Solutions for Large-Amplitude Ship Motions in

the Time-Domain," *Proceedings of the Eighteenth Symposium of Naval Hydrodynamics*, The University of Michigan, U.S.A., 1990

[13] Lin, W.M., and Yue, D.K.P., "Time-Domain Analysis for Floating Bodies in Mild-Slope Waves of Large Amplitude," *Proceedings of the Eighth International Workshop on Water Waves and Floating Bodies*, Newfoundland, Canada, 1993.

[14] Lin, W.M., Zhang, S., Weems, K., and Yue, D.K.P., "A Mixed Source Formulation for Nonlinear Ship-Motion and Wave-Load Simulations," *Proceedings of the Seventh International Conference on Numerical Ship Hydrodynamics*, Nantes, France, 1999.

[15] France, W., Levadou, M., Treakle, T., Pauling, J., Michel, R., and Moore, C., "An Investigation of Head-Sea Parametric Rolling and its Influence on Container Lashing Systems," *Marine Technology*, Vol. 40, No.1, January 2003.

[16] Zhou, Z.Q., De Kat, J.O., and Buchner, B., "A Nonlinear 3-D Approach to Simulate Green Water Dynamics on Deck," *Proceedings of 7th Numerical Simulation Hydrodynamics*, 1999.

[17] Buchner, B., "On the Impact of Green Water Loading on Ship and Offshore Unit Design," *Proceedings of the Sixth Symposium on Practical Design of Ships and Mobile Units*, pp.1.430-1.443. 1995.

[18] Stoker, J.J., "Water Waves," Pure and Applied Mathematics, Vol. 9, The Mathematical Theory and Applications, Institute of Mathematical Sciences, New York University, U.S.A., pp. 22-25, 1957

[19] Liut, D., Weems, K., and Lin, W.M., "Nonlinear Green Water Effects On Ship Motions and Structural Loads," *Proceedings of the 24th Symposium on Naval Hydrodynamics*, Fukuoka, Japan, 2002

[20] Garkavy, V. V., "Deterministic chaos in the task of the roll motion ship with a small freeboard," *Proc. of HADMAR'91: International Symposium On Hydro- And Aerodynamics In Marine Engineering*, Paper 49, Vol. 2, Bulgarian Ship Hydrodynamics Centre, Varna, Bulagria, 1991.

[21] Nayfeh, A. H., and Sanchez, N. E., "Stability and complicated rolling response of ships in regular beam seas," *International Shipbuilding Progress*, Vol. 37, No 412, pp. 331-352, 1990.

[22] Shin, Y.S, Belenky, V.L., Lin, W.M., Weems, K.M., Engle, A.H., "Nonlinear Time Domain Simulation Technology for Seakeeping and Wave-Load Analysis for Modern Ship Design" *to be presented at SNAME Annual Meeting,* San-Francisco, U.S.A. 2003